Biophysical Journal, Volume 98

Supporting Material

Mechano-Chemical Feedbacks Regulate Actin Mesh Growth in Lamellipodial Protrusions

Longhua Hu and Garegin A. Papoian

Supplemental Information: Mechano-Chemical Feedbacks Regulate Actin Mesh Growth in Lamellipodial Protrusions

Longhua Hu[†] and Garegin A. Papoian[1†]

[†]Department of Chemistry, University of North Carolina, Chapel Hill

[1]Correspondence should be addressed to GAP. Email: gpapoian@unc.edu

1 Model details

In our model, the simulation region is partitioned into compartments. The typical size of the simulation region is $5\mu m \times 1\mu m \times 200nm$. Unlike Brownian dynamics studies of cell motility (1–3), we do not explicitly consider the interactions between the molecules and the exact position of each molecule, instead we apply the coarse-grained technique adopted in the simulations of actin filaments growth (4, 5) and partition the whole simulation region into compartments. The size of these compartments is determined from the so-called Kuramoto length (6), which is the typical length over which a molecule diffuses before reacting and can be estimated from $l = \sqrt{6D\tau}$, where τ is average time interval between two consecutive reactions and $D = 20\mu m^2/s$ is the diffusion coefficient of actins. Given that the polymerization is typically the fastest reaction event in our simulation, the shortest time scale is estimated from $\tau = \frac{1}{k_{on}[A]}$, where $k_{on} = 11.6\mu M^{-1}s^{-1}$ is the polymerization rate constant and $[A]$ is monomeric actin concentration. With $[A] = 50\mu M$, we get $l \approx 450nm$. Practically, we set $l = 100nm$ in our simulation. Therefore, the size of the compartments is set as $100nm \times 100nm \times 100nm$. Since the volume of the compartment is fixed ($10^{-3}\mu m^3$), the conversion relationship between the concentration and the number of particles per compartment can be easily obtained. In particular, $10\mu M$ concentration corresponds to about 6 molecules per compartment.

Let's denote the molecules of actin, capping protein and Arp2/3 as A, C and R, respectively, then the reactions in the simulated system can be schematically described by the following:

$$F_n + A \quad \leftrightarrows \quad F_{n+1} \tag{1}$$

$$F_n + C \quad \leftrightarrows \quad F_nC \tag{2}$$

$$F_n + A + R \quad \leftrightarrows \quad F_n + F_1 \tag{3}$$

where F_n represents a filament of length n and F_nC denotes a filament of length n capped by a

capping protein. Eq. (1) shows the polymerization/depolymerization reactions. Eq. (2) shows the capping/uncapping reactions. When the barbed end of a filament is capped by the capping protein, the filament cannot polymerize unless the capping protein is removed due to an uncapping reaction. Eq. (3) shows the nucleation of new filament F_1 on existing filament F_n. Nucleation requires the Arp2/3 and actin. The rates of the forward and backward reactions used in our simulations are summarized in the table in the main text.

Compartments in three-dimensional space may be denoted with the notation (i_x, i_y, i_z), then the diffusions of a molecule M (actin, capping protein and Arp2/3) can be schematically written as

$$M_{(i_x,i_y,i_z)} \leftrightarrows M_{(i_x\pm1,i_y\pm1,i_z\pm1)} \ , \tag{4}$$

which simply means that a molecule M can diffuse to the nearest neighboring compartment as allowed by the geometry of the simulated system.

The rear part of the diffusive region is coupled to the bulk. The exchange of molecules between the bulk and the diffusive part can be written as

$$M_{bulk} \leftrightarrows M_{(ix_0,iy,iz)} \ , \tag{5}$$

where ix_0 is the x-direction index of the compartments coupled to the bulk. With the growth of the filamentous network, ix_0 advances correspondingly. Adjusting the molecular exchange rate between the bulk and the diffusive region would allow particular concentrations of the diffusive region to be achieved.

The coordinate system in our simulations is fixed, where polymerizing actin filaments remain stationary relative to these coordinates. This indicates that we neglect the retrograde flow and assume no slipping of actin filaments, an assumption which is consistent with prior experimental study on a keratocyte lamellipodium (7). We set the substratum in $x - y$ plane with x as motion direction. Positions of filamentous monomers could be represented with either the Cartesian

coordinates (x, y, z) or the spherical coordinates (r, θ, ϕ).

We also assume that filaments are straight and rigid. In our simulations, filaments are typically no more than a few microns in length, much shorter than the persistence length of actin filaments, which is about $16\mu m$ (8). By adopting the straight and rigid filaments approximation, we neglect the elastic energy of the filaments. It is possible that actin filaments would bend or even buckle (9), especially when they experience high protrusion resistance. Such issues will be addressed in future work. In this work, we mainly focus on the chemical aspect of the mecho-chemical regulation of lamellipodial protrusion.

Unlike some works (10, 11), we ignore the nucleotide status of actins because we are interested in the reaction front in the immediate neighborhood of the lamellipodial leading edge.

The plasma membrane is generally considered to be a two-dimensional elastic sheet, commonly described with Monge representation (12). We write the protrusion position x at membrane point (y, z) as $x = x(y, z)$. Because lamellipodia are flat (with thickness $\sim 200nm$), we approximate the front membrane configuration as $x = x(y, z) \equiv x(y)$. That is, we ignore the height difference (z) at each position (y) along the membrane. This makes it possible to represent the front membrane as an effective one-dimensional curve, which then can be characterized using B-spline technique, in which the different shapes of a curve can be realized by moving the control points (for an introduction to B-spline, see, for example (13)). Such an approximation allows for great computational efficiency yet retaining physical relevance of the desired flexible plasma membrane, in contrast to the rigid surface approximation used in many previous computational works (2, 14). Our approach is similar to the Bezier curve representation used in a prior simulation work (15). Other common techniques of representing the membrane include the fluctuating membrane (16) and the finite element method (17, 18).

With the Monge representation $h(y)$ of the membrane, the Helfrich Hamiltonian for the mem-

brane is given by, (12):

$$\begin{aligned} E_m &= \frac{k_b}{2}\int \left(\nabla^2 h(y)\right)^2 dy + \frac{\gamma}{2}\int \left(\nabla h(y)\right)^2 dy \\ &+ \beta \int h(y) dy \,, \end{aligned} \tag{6}$$

where k_b is the bending rigidity and γ is the surface tension coefficient. In our simulation, $k_b = 100 k_B T$ and $\gamma = 0.5 k_B T$. Lamellipodial protrusion is expected to be countered by both internal resistance, due to increasing the membrane area, and also by external obstacles. The last term in Eq. (6) reflects the combined effect due to internal and external forces. That is, the membrane is subject to an external "field" with strength β, which is the combined resistive force per unit length. Throughout the simulation, we used $\beta = 10 pN/\mu m$.

The plasma membrane is confined by the actin filaments, and this physical confinement restricts the conformations the membrane can have. We model the confinement by assuming that there is a repulsive interaction between actin filaments and the membrane. For simplicity, we further assume that the interaction exists only between the barbed ends of actin filaments and the membrane. Such an approximation is justified because in the dendritic array network of the filaments, generally it is the barbed ends of the filaments that are the closest to the membrane. We choose the potential energy in the exponential form:

$$E_{fm} = E_0 \exp\left(-\frac{l}{\lambda}\right) \,, \tag{7}$$

where l is the distance between the barbed end of a filament and the membrane, and λ is the characteristic distance. A barbed end below the membrane ($l > 0$) is energetically favorable. But if the barbed end penetrates the membrane ($l < 0$), the interaction energy significantly increases, making such a position unlikely. The effect of the obstacle on the rate of polymerization can be seen from this term. The external load from obstacle tends to push the membrane closer to the actin filaments, thus decreases the distance l and makes the interaction between membrane and

actin filaments stronger. With the larger force, $f = -\frac{\partial E_{fm}}{\partial l}$, the mechanical work w done for an actin monomer to be added to a filament becomes higher, thus it becomes energetically unfavorable for a polymerization to occur. The exact values of E_0 and λ are not very important: we chose $E_0 = k_B T$ and $\lambda = 0.1\delta << \delta \equiv 2.7nm$, which are effectively able to prevent the filaments from penetrating membrane while contributing a negligible potential energy when all the filaments are below the membrane, as desired. The potential in Eq. (7) represents the repulsive force. We do not consider an additional attractive force, which would exist from the tethering of filaments to the membrane or membrane proteins (19, 20). Physical confinement of the plasma membrane by the filaments and the need to advance membrane due to actin polymerization necessitate the introduction of a repulsive potential. An attractive force is not essential to our simulation model since the membrane is subject to an external field which keeps it from drifting away from the filaments despite the repulsive interaction, which are short range. Hence, the attractive force could be considered as having been absorbed in the external field term. Therefore, in our current model it is not highly essential to have a separate attractive force term. Hence, for simplicity, we neglected a separate attractive energy term in total Hamiltonian. However, besides the mechanical aspect, filament tethering to the plasma by proteins such as N-WASP could have some other interesting effects such as guiding the filament growth. Such topics are very interesting but are beyond the scope of this paper.

We apply periodic boundary condition on the direction perpendicular to the motion direction (y direction), namely, when a filament grows out of boundary, we translate the corresponding filament section to the other side of the periodic cell. The boundaries $h(y = 0)$ and $h(y = y_{max})$ of the membrane are not completely independent due to the periodic boundary condition. To simulate this constraint, we consider that the two boundary points are elastically connected and model this by introducing an elastic potential energy:

$$E_{pbc} = \frac{1}{2} k_{pbc} \left(h(y = 0) - h(y = y_{max}) \right)^2 \ , \tag{8}$$

where $k_{pbc} = 25k_BT$.

With the energy terms described above, we have established the total Hamiltonian: $\mathcal{H} = E_m + E_{fm} + E_{pbc}$. During simulation, when the membrane is perturbed by the filaments due to polymerization, the equilibrium membrane configuration is obtained by minimizing the Hamiltonian. This is justified because of the separation of time scales between polymerization and membrane dynamics. For a concentration of $10\mu M$ actin, the rate of polymerization is about $100s^{-1}$, which means that on average, the time interval between two consecutive polymerization events is about $10ms$, much longer that the typical membrane equilibration time, which is on the order of ns to μs (21).

The membrane described above constitutes the front part of the model lamellipodium. During simulations, the position of the rear part of the lamellipodia is also adjusted, when needed, to keep the total length of the model lamellipodium nearly constant: the segment of any filament below the rear part of the lamellipodium is considered "depolymerized". Thus, we model the disassembly process of the filamentous network in an implicit way. Unless otherwise noted, the length of the model lamellipodia in our simulations is around $1\mu m$.

We have ignored the nucleotide status of the filamentous actins and modeled the depolymerization process in an implicit way, thus our model doesn't include the severing effect by ADF/cofilin proteins, which predominantly bind to ADP-actin filaments and promote the disassembly of actin filaments (22, 23). It is expected that actin dynamics with the presence of ADF/cofilin would depend on its concentration, especially the concentration relative to that of capping protein because this determines whether the newly generated barbed ends would grow to protrude or provide new branching sites (24). ADF/cofilin would affect filamentous network structure, based on prior works that have shown that the severing effect impacts the length distribution of filaments in the filamentous network (25–28). However, in a growing lamellipodium, severing would mainly occur away from the leading edge, where ATP-actin turns into ADP-actin. In this work, we are primarily interested in physico-chemical processes occurring at the leading edge.

During simulations, we record the time trajectories of the position of the traveling front of the model lamellipodia and the number of filaments in the actin mesh, from which we calculate the steady-state protrusion speed and the rate of nucleation. The orientations of filaments as well as their branching states are also recorded, which allows us to construct the full filamentous network at any time snapshot. Other quantities of interest include the capping status of each filament and the number of G-actin, Arp2/3 and capping proteins in each compartment.

References

1. Lee, K.-C., and A. J. Liu. 2008. New proposed mechanism of actin-polymerization-driven motility. *Biophys. J.* 95:4529–4539.

2. Gopinathan, A., K.-C. Lee, J. M. Schwarz, and A. J. Liu. 2007. Branching, capping and severing in dynamic actin structures. *Phys. Rev. Lett.* 99:058103.

3. Jeon, J., N. R. Alexander, A. M. Weaver, and P. T. Cummings. 2008. Protrusion of a virtual model lamellipodium by actin polymerization: a coarse-grained langevin dynamics model. *J. Stat. Phys.* 133:79–100.

4. Lan, Y., and G. A. Papoian. 2008. The stochastic dynamics of filopodial growth. *Biophys. J.* 94:3839–3852.

5. Zhuravlev, P. I., and G. A. Papoian. 2009. Molecular noise of capping protein binding induces macroscopic instability in filopodial dynamics. *Proc. Natl. Acad. Sci. USA* 106:11570–11575.

6. van Kampen, N. G. 1992. Stochastic processes in physics and chemistry. North-Holland, Amsterdam.

7. Theriot, J. A., and T. J. Mitchison. 1991. Actin microfilament dynamics in locomoting cells. *Nature* 352:126–131.

8. Boal, D. H. 2002. Mechanics of the cell. Cambridge University Press, Cambridge.

9. Howard, J. 2001. Mechanics of motor proteins and the cytoskeleton. Sinauer Association, Inc, Sunderland, Massachusetts.

10. Ditlev, J. A., N. M. Vacanti, I. L. Novak, and L. M. Loew. 2009. An open model of actin dendritic nucleation. *Biophys. J.* 96:3529–3542.

11. Halavatyi, A. A., P. V. Nazarov, S. Medves, M. van Troys, C. Ampe, M. Yatskou, and E. Friederich. 2009. An integrative simulation model linking major biochemical reactions of actin-polymerization to structural properties of actin filaments. *Biophys. Chem.* 140:24–34.

12. Safran, S. A. 1994. Statistical thermodynamics of surface, interfaces, and membranes. Addison-Wesley.

13. Marsh, D. 2005. Applied geometry for computer graphics and CAD. Springer, London.

14. Carlsson, A. E. 2001. Growth of branched actin networks against obstacles. *Biophys. J.* 81:1907–1923.

15. Schaus, T. E., E. W. Taylor, and G. G. Borisy. 2007. Self-organization of actin filament orientation in the dendritic-nucleation/array-treadmilling model. *Proc. Natl. Acad. Sci. USA* 104:7086–7091.

16. Daniels, D. R., D. Marenduzzo, and M. S. Turner. 2006. Stall, spiculate, or run away: the fate of fibers growing towards fluctuating membranes. *Phys. Rev. Lett.* 97:098101.

17. Atilgan, E., D. Wirtz, and S. X. Sun. 2005. Morphology of the lamellipodia and organization of actin filaments at the leading edge of the crawling cell. *Biophys. J.* 89:3589–3602.

18. Rubinstein, B., K. Jacobson, and A. Mogilner. 2005. Multiscale two-dimensional modeling of a motile simple-shaped cell. *Multiscale Model. Simul.* 3:413–439.

19. Mogilner, A., and G. Oster. 2003. Force generation by actin polymerization ii: the elastic ratchet and tethered filaments. *Biophys. J.* 84:1591.

20. Co, C., D. Wong, S. Gieke, V. Chang, and J. Taunton. 2007. Mechanism of actin network attachment to moving membranes: barbed end capture by n-wasp wh2 domains. *Cell* 128:901–913.

21. Gov, N. S., and S. A. Safran. 2005. Red blood cell membrane fluctuations and shape controlled by atp-induced cytoskeletal defects. *Biophys. J.* 88:1859–1874.

22. Pollard, T. D., and G. G. Borisy. 2003. Cellular motility driven by assembly and disassembly of actin filaments. *Cell* 112:453–465.

23. Pollard, T. D., and J. Berro. 2009. Mathematical models and simulations of cellular processes based on actin filaments. *J. Biol. Chem.* 284:5433–5437.

24. Andrianantoandro, E., and T. D. Pollard. 2006. Mechanism of actin filament turnover by severing and nucleation at different concentrations of adf/cofilin. *Molecular Cell* 24:13–23.

25. Carlsson, A. E. 2006. Simulation of actin polymerization by filament severing. *Biophys. J.* 90:413–422.

26. Edelstein-Keshet, L., and G. B. Ermentrout. 2001. A model for actin-filament length distribution in a lamellipod. *J. Math. Biol.* 43:325–355.

27. Roland, J., J. Berro, A. Michelot, L. Blanchoin, and J.-L. Martiel. 2008. Stochastic severing of actin filaments by actin depolymerizing factor/cofilin controls the emergence of steady dynamical regime. *Biophys. J.* 94:2082–2094.

28. Huber, F., J. Kas, and B. Stuhrmann. 2008. Growing actin networks form lamellipodium and lamellum by self-assembly. *Biophys. J.* 95:5508–5523.

29. Pollard, T. D. 1986. Rate constants for the reactions of atp-and adp-actin with the ends of actin filaments. *J. Cell. Biol.* 103:2747–2754.

30. Mogilner, A., and L. Edelstein-Keshet. 2002. Regulation of actin dynamics in rapidly moving cells: a quantitative analysis. *Biophys. J.* 83:1237–1258.

Table S1: Reaction and diffusion parameters are listed. Rates in parentheses are recalculated corresponding to the specific compartment size in our simulations.

Reactions	Forward reaction rate	Backward reaction rate (s^{-1})	Refs
Polymerization	11.6 $\mu M^{-1}s^{-1}$ (19.3/s)	1.4	(29)
Capping	3.98 $\mu M^{-1}s^{-1}$ (6.6/s)	0.04	(5)
Nucleation	8 $\mu M^{-2}s^{-1}$	0.05	this article
Diffusion	20 $\mu m^2/s$ (2000 s^{-1})	2000	(30)

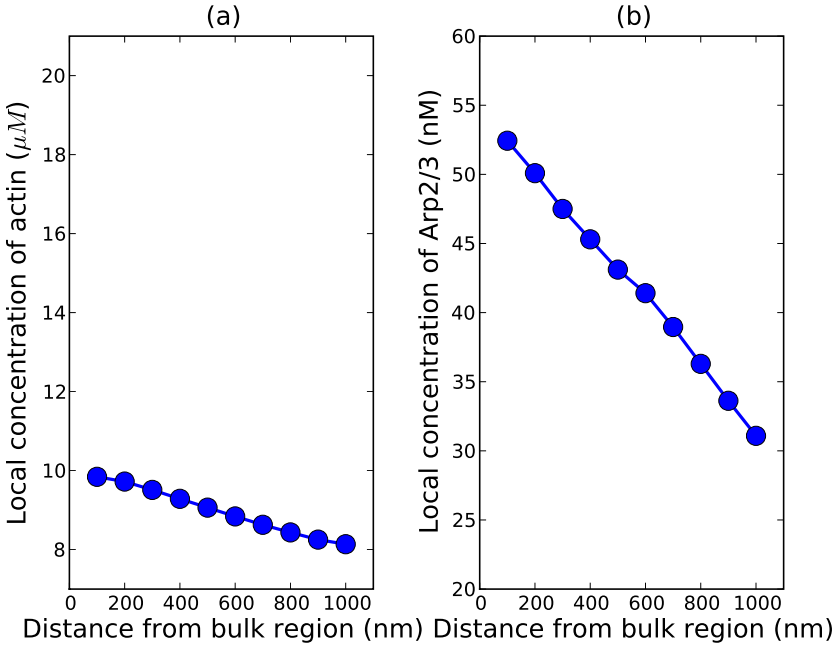

Figure S1: Spatial profile of the concentrations of actin (a) and Arp2/3 (b). There is a concentration gradient from the bulk region at the rare to the membrane in front. The bulk concentrations of actin, capping proteins and Arp2/3 are $10\mu M$, $50nM$ and $50nM$, respectively.

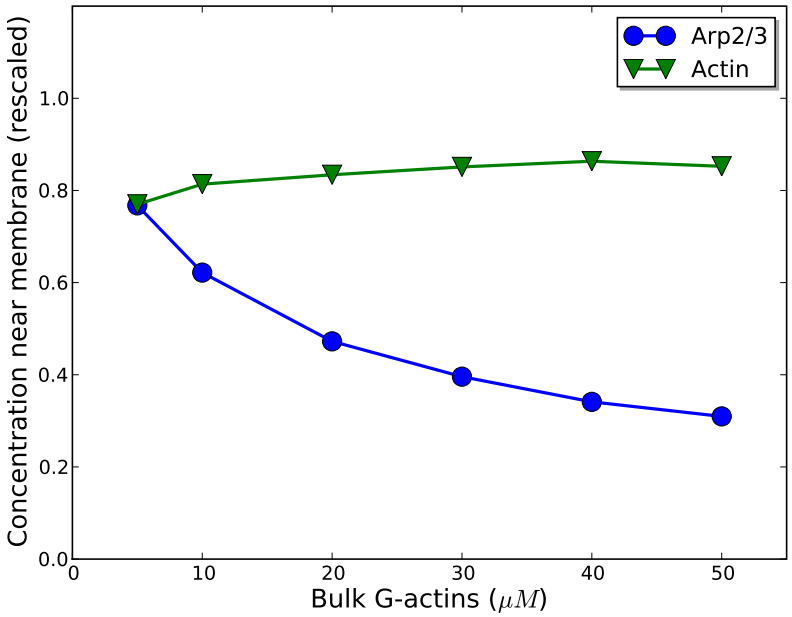

Figure S2: Dependence of local concentrations of Arp2/3 and actin near the membrane on bulk G-actin concentration. With the increase of bulk G-actins, there is an increase of actin concentration and a decrease of Arp2/3 concentration near membrane. Note the concentrations of Arp2/3 and actin near membrane are rescaled relative to their corresponding bulk values at each point. The bulk concentration of Arp2/3 is kept constant.

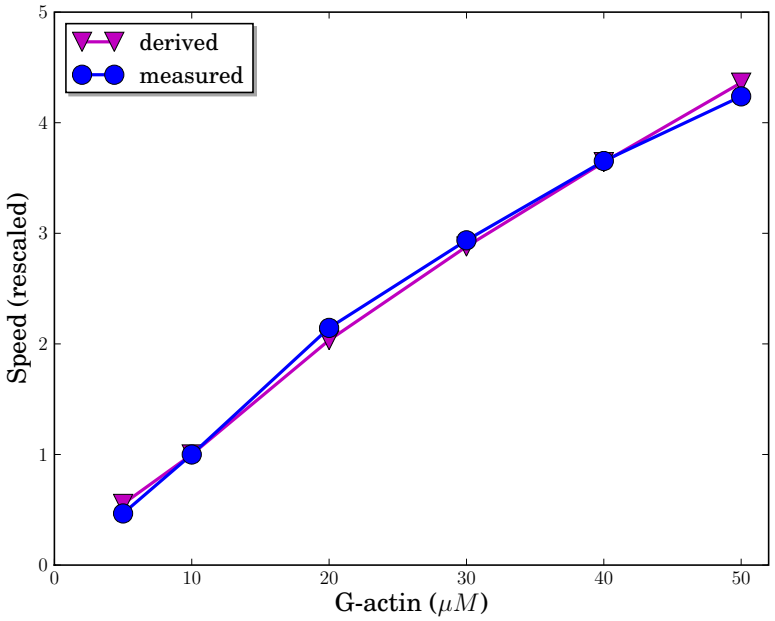

Figure S3: Protrusion speeds obtained from simulations and estimated from the average load and average local concentration of actin, using $\chi k_{on}\langle[A]\rangle\delta e^{-\langle w\rangle/K_BT}$ with scaling factor $\chi \approx 0.63$, which is the average projection of unit length $\langle sin(\theta)cos(\phi)\rangle$ along motion direction resulting from various orientations of polymerizing filaments. The absolute magnitudes are uniformly rescaled to facilitate the comparison between two curves and show the overall trend.

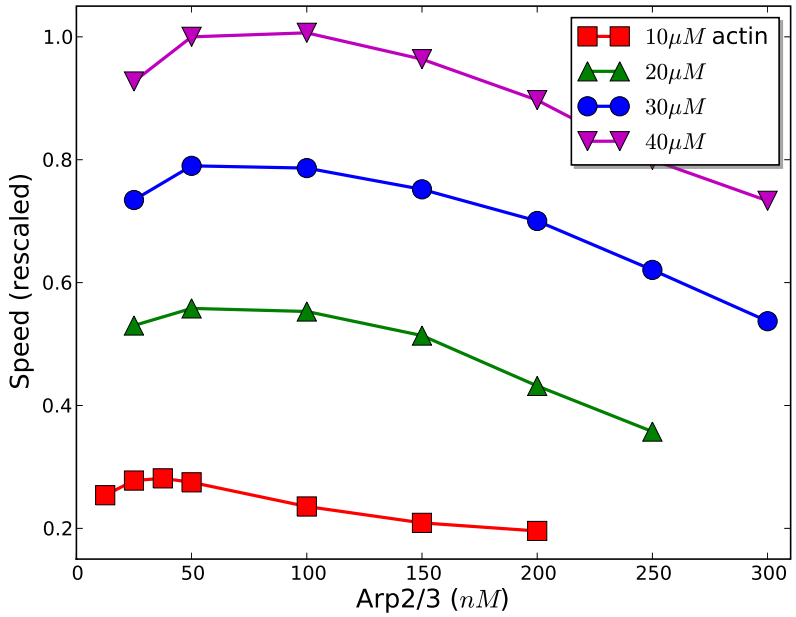

Figure S4: Protrusion speeds derived from the average load and average local concentration of G-actins available for polymerization, based on $\chi k_{on}\langle[A]\rangle\delta e^{-\langle w\rangle/K_BT}$ with scaling factor $\chi \approx 0.76$, show non-monotonic dependence on Arp2/3 concentration. The speeds are uniformly rescaled to show the overall trend.

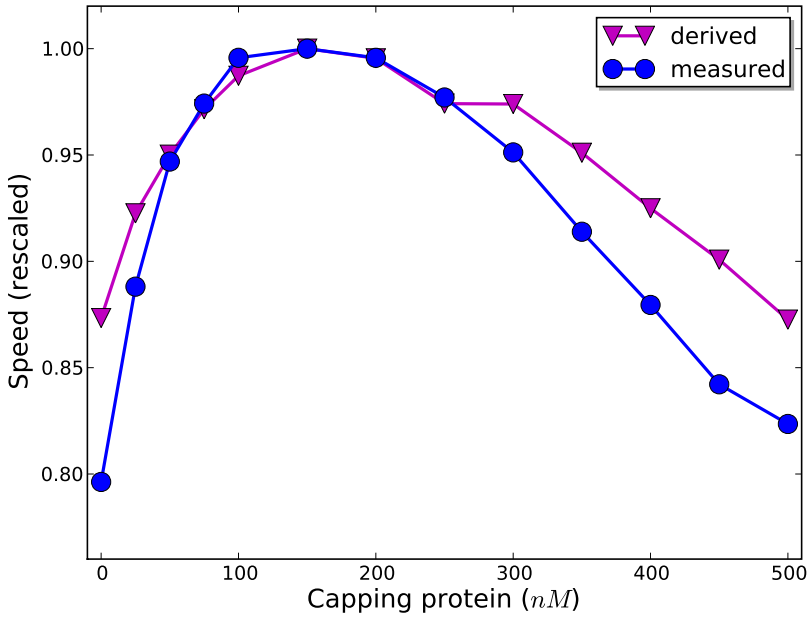

Figure S5: Protrusion speed obtained from simulations and estimated from averaged quantities, using $\chi p k_{on} \langle [A] \rangle \delta e^{-\langle w \rangle / K_B T}$ with scaling factor $\chi \approx 0.53$. The speeds shown here are rescaled with respect to the maxima to facilitate the comparison between two curves.